Contribution of Longitudinal GFRP Bars in Concrete Cylinders under Axial Compression

Brandon Fillmore and Pedram Sadeghian[1]

Department of Civil and Resource Engineering, Dalhousie University, 1360 Barrington Street, Halifax, NS, B3H 4R2, Canada.

Abstract: Contribution of longitudinal glass fiber-reinforced polymer (GFRP) bars in concrete columns under compression has been ignored by current design guidelines. This paper challenges this convention by testing 21 concrete cylinders (150 mm × 300 mm) reinforced with longitudinal GFRP and steel bars in compression. It was observed that GFRP bars could sustain high level of compressive strains long after the peak load of the specimens without any premature crushing. The results of a new coupon test method showed that the elastic modulus of GFRP bars in compression is slightly higher than that of in tension, however the compressive strength was obtained 67% of tensile strength. An analytical model was successfully implemented to predict the axial capacity of the tests specimens and it was found that the contribution of the bars in the load capacity of the specimens was within 4.5-18.4% proportional to the bars reinforcement ratio normalized to the elastic modulus of steel bars.

Keywords: GFRP, Reinforcing Bar, Compression, Crushing, Contribution.

1. INTRODUCTION

Using fiber-reinforced polymer (FRP) bars and especially glass FRP (GFRP) to reinforce concrete structures has become increasingly common in the past three decades. The corrosion resistant

[1] Corresponding Author. Email: Pedram.Sadeghian@dal.ca

nature of GFRP bars against de-icing salt, ocean water, and other harsh environments has been the main advantage over steel bars and therefore the use of GFRP bars would be of great benefit in many structural applications. Moreover, GFRP bars' high strength and light weight within reasonable cost are other advantages. The application of longitudinal GFRP bars in concrete beams and slabs as tensile reinforcement has been relatively established (Nanni 1993, Benmokrane et al. 1995, El-Sayed et al. 2005, and Bischoff 2005). However, the use of longitudinal GFRP bars in concrete columns has been very limited. The topic of whether to include the compressive contribution of longitudinal GFRP bars in the calculation of column capacity has been a subject of discussion.

In a study by De Luca et al. (2010), longitudinal GFRP bars were found to contribute from 2.9% to 4.4% to the capacity of large-scale axially loaded columns which compared to an 11.6% contribution by longitudinal steel bars with the same reinforcement ratio of 1%. This study concluded that the axial capacity can be computed neglecting the contribution of the internal GFRP reinforcement and considering the only force carried by the concrete. Pantelides et al. (2013) tested medium-scale concrete columns and found that the axial capacity of columns reinforced with 1.6% longitudinal GFRP bars achieved 84% of the axial capacity of control column reinforced with 1.0% steel bars. It was concluded that columns must be reinforced with a larger reinforcement ratio GFRP bars to achieve a similar performance of control columns.

On the other hand, several other experimental studies have demonstrated a significant contribution of longitudinal GFRP bars in concrete columns. Tobbi et al. (2012) tested large-scale columns and reported that GFRP bars contributed 10% of column capacity, which is close enough to steel's contribution (12%). It was concluded that GFRP bars could be used in compression members if adequate transverse bars provide to eliminate bar buckling. Tobbi et al. (2014)

expanded the previous study and investigated concrete columns reinforced longitudinally with GFRP, carbon FRP (CFRP), and steel bars plus GFRP and CFRP transverse reinforcement. It was concluded that the contribution of longitudinal FRPs in concrete columns subjected to axial concentric loading should not be neglected. Also, Afifi et al. (2013) tested 12 full-scale circular concrete columns reinforced with longitudinal GFRP bars under concentric axial loads and concluded that ignoring the contribution of GFRP bars in design equation underestimated the maximum capacity of the tested specimens.

Recently, Karim et al. (2016) and Hadhood et al. (2017) tested GFRP-reinforced concrete columns under combined axial load and bending moment. Karim et al. (2016) found that longitudinal GFRP bars improved the peak load and the ductility of the columns. Hadhood et al. (2017) reviewed and discussed the compressive contribution of GFRP bars and found that ignoring the contribution of the compression GFRP bars underestimated the nominal axial load and moment capacity of the tested columns (27% on average). Integrating the contribution of the compression GFRP bars, however, returned a more reasonable estimation (17% on average). Moreover, Hadi et al. (2016) and Maranan et al. (2016) studied the effect of hoops and spirals reinforcements with different spacing on the behavior of GFRP-reinforced concrete columns.

Design guidelines including ACI 440.1R (2015) and CAN/CSA S806 (2012) currently neglect the compressive contribution of GFRP bars. The approach has been rooted in concerns surrounding the compressive strength and elastic modulus of GFRP bars and the possibility of premature failure of the bars in compression. For example, per ACI 440.1R (2015), the contribution of FRP bars should be neglected when used as reinforcement in columns, in compression members, or as compression reinforcement in flexural members. However, it is acceptable for FRP tension reinforcement to experience compression due to moment reversals or

changes in load pattern. It is believed that the maximum contribution of compression FRP bars calculated at ultimate concrete strain (typically at ε_{cu} = 0.003) is small due to: (i) the relatively lower elastic modulus of FRPs compared with steel; and (ii) the lower elastic modulus of FRP bars in compression as compared to tension. The authors of this paper believe the first reasoning is logical for GFRP bars as majority of GFRP bars in the market have an elastic modulus ranging from 40 to 60 GPa (20 to 30% steel's elastic modulus). However, the effect of low modulus can be calculated based on elastic theory as proposed by Tobbi et al. (2014). The axial capacity of a concrete column reinforced with longitudinal FRP bars can be calculated as follows:

$$P_n = 0.85 f'_c\left(A_g - A_f\right) + \varepsilon'_c E_{fc} A_f \quad (1)$$

where P_n is the nominal axial capacity, f'_c is the concrete compressive strength, ε'_c is the strain of concrete at peak load (typically taken as 0.002 mm/mm), A_g is the gross cross-sectional area, A_f is the area of longitudinal FRP bars, and E_{fc} is the elastic modulus of FRP bars in compression. It should be highlighted that the concrete compressive strength f'_c is based on 150 mm × 300 mm standard cylinders. Per Hognestad (1951), it is not applicable for concrete columns and the maximum stress of 0.85 f'_c was proposed. This value was found as an average in numerous tests of vertically-cast concentrically loaded columns. Effects of size and shape of the columns as well as of the casting position was included in the factor 0.85. In this paper, concrete cylinders were tests and as s results the factor 0.85 is not considered. The second term in Equation (1) corresponds to the contribution of longitudinal FRP bars at the peak load. If the elastic modulus of FRPs in compression was less than tension one, it would be considered automatically.

As there is no standard test method for FRP bars in compression, there are multiple and even controversial opinions in the literature regarding the strength and elastic modulus of FRP bars in compression. De Luca et al. (2010) specified that testing of FRP bars in compression is typically

complicated by the occurrence of fiber micro-buckling due to the anisotropic and non-homogeneous nature of the FRP material, and can lead to inaccurate measurements. Therefore, standard test methods are not established yet. For the case of GFRP bars, reductions in the compressive strength and elastic modulus by up to 45 and 20% with respect to the values in tension, respectively, have been reported (De Luca et al. 2010). Deitz et al. (2003) tested GFRP bars (15 mm diameter) in compression with unbraced length of 50 to 110 mm (length/diameter of 3.3 to 6.7). The test results indicated that the compressive strength of the bars was varied from about 50 to 120% (average = 85%) of the tensile strength. Moreover, the elastic modulus showed to be the same in compression and tension. On the other hand, Tobbi et al. (2014) concluded that the ultimate axial compressive strain for columns reinforced longitudinally and transversally with FRP bars can reach a value on the same order of magnitude as the FRP ultimate tensile strain of the longitudinal bars under good confinement conditions.

The lack of consensus and clear understanding surrounding the compressive behavior of GFRP reinforcement means that more research is required to understand their behavior, especially in concrete. This paper is a part of a comprehensive project on behavior of longitudinal FRPs as internal and external reinforcements of short and long concrete specimens under concentric and eccentric loading. Fillmore and Sadeghian (2017) applied additional fiberglass threads spirally around GFRP bars and studied its effect on the compressive behavior of the bars in concrete cylinders comparing with GFRP bars without the spiral threads, briefly. Moreover, Khorramian and Sadeghian (2017a, 2017b, and 2017c) studied the compressive behavior longitudinal FRPs in small-scale concrete specimens with square cross-section under combined axial and bending moment.

This paper aims to examine how GFRP bars behave in short reinforced concrete cylinders under concentric loading. Analyzing the compressive behavior GFRP bars at this level is fundamental to understanding the failure mechanism of the bars surrounded with concrete. The test data is implemented to quantify the contribution of GFRP bars when concrete reached to its peak stress. For this reason, several concrete cylinders were reinforced with steel and GFRP bars and testes under axial compressive loading up to failure. The number of bars was varied to establish a meaningful comparison for different reinforcement ratios. The load capacity and toughness of the specimens and strain of the bars were compared and the contribution of bars at peak load was obtained. An analytical study was also performed on the load capacity and verified with the experimental data. Also, a new test method is proposed to determine the compressive properties of GFRP bars.

2. RESEARCH SIGNIFICANCE

The use of GFRP bars as tensile internal reinforcement of concrete structures has become popular, especially for beams and slabs. However, there is a concern in the literature regarding application of GFRP bars in compression. North American design guidelines including ACI 440.1R (2015) and CAN/CSA S806 (2012) currently neglect the compressive contribution of GFRP bars in beams and columns. It is commonly believed that GFRP bars are not as effective as steel bars in load bearing capacity of concrete columns. The approach has been rooted in concerns surrounding the compressive strength and elastic modulus of GFRP bars and the possibility of premature failure of the bars in compression. In addition, the lower elastic modulus of GFRP bars with respect to steel bars has magnified the concern. This study was designed to investigate compressive behavior of

GFRP bars in concrete. Moreover, it proposes a new test method of testing GFRP bar coupons in compression.

3. EXPERIMENTAL PROGRAM

Several concrete cylinders were reinforced with steel and GFRP bars and testes under axial compression. This section presents the details of the experimental program including specimen layout, material properties, specimen preparation, test set-up and instrumentation.

3.1. Specimen Layout

A total of 21 concrete cylinders with a diameter of 150 mm and a height of 300 mm were prepared and tested under uniaxial compressive loading. As shown in Table 1, the testing matrix included 7 groups of specimens, namely, plain (unreinforced/control), steel-reinforced concrete specimens (3 groups), and GFRP-reinforced concrete specimens (3 groups). Reinforced specimens were built in 4, 6, and 8 bar arrangements with axisymmetric distribution. Three identical specimens were prepared for each group. The specimen identification (ID) numbers consist of a two-part naming system "X-N": the first part "X" being the type of reinforcing bar, namely "P" (Plain, no reinforcement), "S" (Steel-reinforced concrete), and "G" (GFRP-reinforced concrete); and the second part "N" being the number of bars arranged in the specimen, namely 4, 6, and 8.

3.2. Material Properties

Concrete was delivered in a ready-mix batch with maximum aggregate size of 12.7 mm and slump of 100 mm. The average compressive strength of concrete at the time of test was 36.2 MPa. The manufacturer's specifications for the GFRP bars (#4) are for a nominal cross-sectional area of 126.7 mm^2 with the tensile properties of peak load, ultimate strength, and elastic modulus being specified as 95.90 kN, 758 MPa and 46 GPa, respectively (manufacturer: Hughes Brothers,

Seward, NE, USA). The steel bars used were 10M (nominal cross-sectional area of 100 mm^2) with a specified tensile strength of 400 MPa and an elastic modulus of 200 GPa.

3.2.1. Tension Coupon Tests

Three GFRP bar specimens were prepared and tested in tension per ASTM D7205/D7205M-06. (2006). Steel tubes were used as end anchors and connected to the GFRP bars using a mixture of epoxy resin and silica sand. Two strain gauges were attached on the surface of the bars at the mid-length of the specimen. Tensile load was applied in a displacement control rate of 2 mm/min. The specimens ruptured in a brittle mode. The average of two strain gauges was used to plots stress-strain curves as shown in Figure 2(a). The average ± standard deviation of the tensile strength, tensile elastic modulus, and tensile rupture strain of GFRP bars were obtained as 839±49 MPa, 44.2±1.7 GPa, and 0.0209±0.0021 mm/mm, respectively. The compressive elastic modulus was calculated based on a chord modulus ranging from a strain of 0.001 to 0.003 mm/mm. It should be noted that the GFRP bars used in this study were available at Dalhousie University from an old batch at the time of the research and were not the latest product of the manufacturer. Also, three steel bar specimens were prepared and tested in tension. The average ± standard deviation of the yield strength of steel bars were obtained as 464±19 MPa.

3.2.2. Compression Coupon Tests

As there is no standard method for testing FRP bars in compression, a new test method proposed by Khorramian and Sadeghian (2017a) was implemented through applying pure compression load on five short GFRP bar specimens with a free length twice the diameter of the bars. To eliminate the stress concentration and premature failure at the ends of bar specimens, two steel caps including a steel hollow cylindrical section with inner diameter of 32 mm and depth of 12.7 mm were used. The caps were filled with a high strength epoxy-based adhesive to fix the rebar specimens. Two

strain gauges were attached on the surface of the bars at mid-length. Compression load was applied with a rate of 2mm/min. For the compression test, a spherical platen was used at the bottom of the specimens to align them with the axis of loading minimizing accidental eccentricities. Mode of failure of rebars in compression test was crushing and no global buckling was observed during the test. It should be highlighted that the test was designed to prevent global buckling of the bars using the length/diameter ration of 2. However, the local buckling of individual fibers at the failure section was observed. Figure 2(b) shows the stress-strain curves of the specimens. The average ± standard deviation of compressive strength, elastic modulus, and ultimate strain of GFRP were obtained as 559 ±36 MPa, 45.5±1.5 GPa, and 0.0122±0.0012 mm/mm, respectively. Figure 2(b) shows the stress-strain diagram obtained from the compression tests. The compressive elastic modulus was calculated based on a chord modulus ranging from a strain of 0.001 to 0.003 mm/mm. The tests set-up and tested specimens are shown in Figure 3.

It was observed that the compressive strength of GFRP bars in compression was 67% of tensile strength. Also, the elastic modulus of GFRP rebar tested in compression was slightly higher than that of in tension, which justify the assumption of having the same elastic modulus in tension and compression. It means ignoring compressive strength of GFRP bars and considering their strength and modulus like concrete in compression is not realistic. It should be noted that the performance of GFRP bars in concrete could be different than coupon test. That is another reason for designing the experimental program

3.3. Specimen Preparation

The dimensions and compressive testing procedure followed ASTM C39M-16 (2016) but with specimen-construction modifications to accommodate and isolate the effects of the GFRP and steel reinforcement. As shown in Figure 1, The reinforcing bars were radially located at equal angles

about the centre of the specimen, such that concrete cover was consistently 25 mm and the clear space between bars was at least 20 mm. Since alignment of the reinforcing was crucial to achieving consistent and meaningful data, a method of specimen preparation was developed to maintain the integrity of the reinforcement geometry throughout the building process.

After applying strain gauges to selected bars as shown in Figure 4(a), the bars were installed in cylindrical plastic molds. Limited space within the 150×300 mm specimen size lead to the development of a method whereby the bars would be end-bearing and keep precise longitudinal orientation without the use of internal ties: this was done by creating a temporary base beneath the mold to support the extruded ends of the bars during consolidation as shown in Figure 4(b). The base functioned as cantilever, holding the bars in place using a rigid polymer-fine aggregate mixture. While the bonding mixture cured in the cantilever base, the bars were braced for proper alignment. This method allowed the faces of the consolidated concrete specimens to be ground smooth such that specimens were able to be axially loaded through a uniform cross section. The cantilever base also proved to be sufficiently strong to maintain the reinforcement alignment during placement and consolidation of the concrete. As shown in Figure 4(c), The fresh concrete was placed and consolidated in two layers using scoops, a vibration table, and then the surface was carefully troweled smooth as shown in Figure 4(d). The consolidated concrete was left in the molds and covered to moist cure for 4 days before the molds were removed and the specimens were relocated to the laboratory to be tested 4 weeks later.

3.4. Test Setup and Instrumentation

As shown in Figure 4(e), deformation of the specimens was measured using three linear variable differential transformer (LVDT) units fixed to the cylinder using a point-bearing yolk: two longitudinal LVDT units with 200 mm gauge lengths were placed on opposite sides to measure

axial deformation while the third measured lateral (i.e. radial) deformation across the full 150 mm diameter until spalling occurred. The reinforced specimens also implemented two 12 mm longitudinal strain gauges each with 6 mm gauge length, which were bonded to flat surfaces machined in-house into the outward facing sides of the bars before pouring concrete. The strain gauges were also protected by a protective coating and covered with aluminum tape. In each reinforced specimen, the two bars with strain gauges were placed in a similar polar opposite arrangement to the longitudinal LVDT units, with the strain gauges facing the outside of the specimens. As shown in Figure 4(f), the compressive testing was done on a 2 MN universal testing frame and was programmed to deform the specimens at a rate of 0.6 mm per minute. The specimens were compressed until either the internal reinforcement began to crush (long after peak load) or until it did not seem safe to deform the specimen any further.

4. EXPERIMENTAL RESULTS AND DISCUSSIONS

Main test results are load capacity and load-strain responses of the specimens. Table 2 presents the summary of test results based on average of three identical specimens of each group. The following sections present the detail of the test results with in-depth discussions on failure modes, the effect of bars on peak load, strain at peak load, toughness, and load-strain diagrams.

4.1. Failure Mode

Figure 5 shows all GFRP- and steel-reinforced specimens after the test. Every specimen exhibited an observable initiation of micro-cracks, causing an audible fracturing in the concrete and development of the longitudinal surface cracks, which had originally appeared approaching peak load. The peak load of steel-reinforced concrete specimens was typically associated with crushing of concrete and yielding of steel bars. When concrete cover was spalled, the steel bar started to

buckle too. For GFRP-reinforced concrete specimens, no GFRP crushing or buckling was observed up to peak load. After the peak load, concrete cover started to spall and gradually bars started to buckle as they lost the lateral support of concrete cover. Few GFRP bars crushed in the process, long after the peak load.

Overall, as shown in Figure 6, after crushing of concrete, three modes of failure were observed, namely, (a) inelastic buckling of steel bars; (b) elastic buckling of GFRP bars; and (c) crushing of GFRP bars. As the buckling of steel bars was inelastic, the steel bars kept a permanent deformed shape after unloading, however buckled GFRP bar were returned to almost original shape after unloading. After the specimens were removed from the testing frame, it became clear that the steel reinforcing separated a concrete core from the exterior concrete which ultimately spalled. The concrete fracturing in most of the steel-reinforced specimens resembled the conical failure of the plain concrete specimens but with the core being protected, except for the 4-bar steel reinforced specimens, where the shear cone permeated the perimeter of the core as defined by the reinforcement bars.

The GFRP-reinforced specimens had similar intragroup trends for 4-, 6-, and 8-bar arrangements to that of the steel group. Since the GFRP bars had greater diameter than that of steel, the difference in the behavior of the 8-bar GFRP reinforced specimens to the 4- and 6-bar arrangements is more profound than in the steel group. The 6-bar GFRP reinforced concrete composite effectively cancelled the independent brittle failure modes of its individual components and resulted in a pseudo-ductile failure mode, albeit with much less of an increase in the peak load compared to a similar steel specimen. The loading of the specimens showed high deformability of GFRP bars for safe post-peak behaviour and considerable resiliency after unloading.

4.2. Effect of Bars on Peak Load

The average peak load of all the specimen groups are shown in Figure 7. In the figure, the error bars illustrate the standard deviation of peak load of 3 identical specimens in each group. The steel bars proved to have larger effect than GFRP bars in increasing the peak load of the cylinders. The 4-bar steel arrangement increased the peak load over plain concrete from 639 kN to 792 kN (24% increase), and further increases to 585 and 911 kN (34 and 43% increase over plain) were made with the 6- and 8-bar steel arrangement, respectively, as shown in Table 2. The 4-bar GFRP arrangement increased the peak load over plain concrete from 639 kN to 709 kN (11% increase), and further increases to 725 kN (13% increase over plain) were made with the 6-bar GFRP arrangement. The 8-bar GFRP arrangement showed an average peak load of 723 kN showing only 2 kN lower than that of 6-bar GFRP arrangement, which is within the standard deviation of the peak load of 8-bar GFRP arrangement (i.e. 25 kN, see Table 2). As shown in Figure 7, GFRP bars are not as effective as steel bars. However, as it is discussed in following sections, the low effectiveness of GFRP bars with respect to steel bars is due to lower elastic modulus not crushing nor buckling.

4.3. Effect of Bars on Strain at Peak Load

As shown in Figure 8, both steel and GFRP bars increased the axial strain at peak load of the specimens, except 8 GFRP bars. The 6-bar specimens increased the strain at peak the most. The strain at peak load of plain specimens were 0.0021 mm/mm and both steel and GFRP bars increased it to an average of 0.0026 (24% increase). According to Equation (1), contribution of GFRP bars is proportional to its elastic modulus in compression and the axial strain at peak load of reinforced concrete. The mechanism is different for concrete reinforced with steel bars, as yielding of steel at typical strain of 0.002 mm/mm marks the maximum resisting force of steel bars. As GFRP bars have linear behavior, more axial strain means more contribution for GFRP

bars. This affects the contribution of GFRP bars in the load capacity. Thus, Equation (2) was adopted from Hognestad (1951) to be used for the strain at peak of the test specimens rather than the conventional value of 0.002 mm/mm.

$$£_c' = 2\frac{f_c'}{E_c} \quad (2)$$

In Equation (2), ε'_c is the strain of concrete at peak load, f'_c is the concrete compressive strength, and E_c is the elastic modulus of concrete. The equation predicts 0.0026 and 0.0027 mm/mm for the strain at peak load of the specimens using the elastic modulus of concrete per ACI 318 (2014) and CAN/CSA A23.3 (2014), respectively, which are compatible with the average experimental value of both steel and GFRP reinforced concrete specimens. It should be highlighted that the validity of Equation (2) for large-scale concrete columns reinforced with GFRP bars should be verified based on large-scale test specimens.

4.4. Effect of Bars on Load-Strain Behavior

The effect of both steel and GFRP bars is demonstrated in the representative load-strain curves comprising Figure 9. Each specimen had two 6 mm axial strain gauges located on the externally-facing shallow-milled surfaces of two reinforcement bars, as well as the two axial LVDTs of 150 mm gauge length. The axial deformation as measured by the LVDTs and the strain gauges were close up to peak load. However, the strain gauge data for steel specimens began to measure higher strains than the LVDTs with further deformation beyond the peak load resistance. Thus, the load-strain curves of the steel-reinforced specimens are based on LVDT data. With the GFRP reinforcement, the difference between the LVDT and strain gauge measurements were minor, and there was almost no difference between the data from each measurement source in the modified GFRP groups. Thus, for the GFRP-reinforced specimens, all 4 measurements (2 strain gauges and 2 LVDTs) were averaged to determine accurate load-strain data for each specimen, then used to

compute the average curve for each group of three identical specimens. This computation process means that each individual curve of GFRP bars in Figure 9 represents the data from 12 axial strain measurements.

Overall, GFRP bars enhanced the peak load and area under the curve of the concrete specimens over plain concrete specimens. However, GFRP bars were not as effective as steel bars. The specimens with 6 GFRP bars resulted in a much broader peak in the load-strain curves, whereas the specimens with 8 GFRP and steel bars showed a sudden drop after the peak load. As shown in Figure 9, the GFRP bars sustained large strains long after the peak load and beyond the crushing strain of 0.0122 mm/mm from coupon compression tests as described in Sec. 2.2. during the tests, few GFRP bars crushed and due to a sudden drop the test was terminated. For example, one of specimens with 8 GFRP bars experienced GFRP crushing as presented in Figure 6(c). The axial strain corresponding to GFRP crushing was larger than the crushing strain of 0.0122 mm/mm from coupon compression tests. It shows that the proposed test method in Sec. 2.2 can capture the crushing strain of GFRP bars close to real condition in concrete.

4.5. Effect of Bars on Toughness

The toughness was computed by numerical integration of the area under the axial load vs. axial strain curve of each specimen. The value was divided by the volume of the cross-section of concrete cylinder to obtain a toughness value with a unit of N-mm/mm^3. In order to make a comparison between toughness of specimens, the procedure numerical integration was terminated when a specimen's load resistance decreased to 85% of its peak load. Figure 10 shows the variation of toughness for the test specimens. Overall, the toughness of GFRP-reinforced specimens was slightly less than that of steel-reinforced specimens. As shown in Table 2 and Figure 10, the only anomaly was the 6-bar GFRP-reinforced specimens, where gradual post-peak behavior of the

specimens resulted in higher axial strain at 85% of peak load. An important distinction between the 8-bar specimens and those with fewer bars is that they showed the least toughness. The 8-bar specimens achieved the highest peak loads within their group, but it came at a price as the high reinforcement ratio led to brittle failure after the peak load was reached. Since the radial distance of the bars is constant throughout all reinforced specimens, the 8-bar reinforcement geometry decreases the concrete-to-concrete bonding area between the core and the cover; which meant that the cover was prone to spalling with transverse expansion through the Poisson's effect. As a result, the 8-bar specimens proved to have a lower toughness than even the 4-bar specimens. These results suggest that there is an optimization of the reinforcement ratio to achieve the maximum toughness. As there was no transverse reinforcements, the unbraced length of bars was slightly less than 300 mm. It means real-size concrete columns with high GFRP reinforcement ratio need to have less spacing of transverse reinforcement preventing buckling of bars and increasing the toughness and energy absorption of the system. Since GFRP bars are linear elastic until crushing at a high strain, their contribution consistently increases until the specimen relies almost entirely on the GFRP bars buried within fractured concrete. The post peak behavior of GFRP-reinforced concrete specimens with high reinforcement ratio can be enhanced with more transverse reinforcements.

4.6. Effect of GFRP Reinforcement Ratio

The reinforcement ratio of specimens reinforced with 4-, 6-, and 8-bar steel arrangements were 2.26, 3.40, and 4.53%; respectively. Also, the reinforcement ratio of specimens reinforced with 4-, 6-, and 8-bar GFRP arrangements were 2.87, 4.30, and 5.74%; respectively. As shown in Figure 7, increasing reinforcement ratio of both steel and GFRP increased the load capacity of the specimens. However, the rate of the increase for GFRP bars was much lower than that of steel bars. This can be explained with lower modulus of GFRP bars. It should be highlighted that there

is a fundamental difference between GFRP-reinforced concrete specimens and steel-reinforced ones. In conventional concrete specimens reinforced with steel bars, peak load of specimens is reached at a strain level close to yielding strain of steel bars. As a result, after the peak load, the stress of steel bars does not increase. However, the story for GFRP bars is different. As GFRP bars are linear elastic, if concrete sustains high strains, the stress of GFRP bars increases until concrete cover spalls and GFRP bars are buckled and/or crushed. This study showed that GFRP bar crushing occurs long after peak load, so the lateral support and spacing of transverse bars are critical. In addition, using high-strength concrete with high strain at peak load will be beneficial, especially with high reinforcement ratio of GFRP bars to increase the contribution of the bars.

5. ANALYTICAL STUDIES

In this section, the axial load capacity of the concrete specimens reinforced with longitudinal GFRP bars and the contribution of the bars in load bearing capacity of the specimens are formulized and the results are compared to the experimental data.

5.1. Load Capacity

The nominal axial capacity of a concrete specimen reinforced with longitudinal FRP bars in compression can be calculated as follows:

$$P_n = P_c + P_f \tag{3}$$

where P_n is the nominal axial capacity, P_c is the concrete contribution, P_f is the FRP contribution. It should be highlighted that the second term corresponds to the contribution of FRP bars at the peak load, not their ultimate capacity in compression. As FRP bars have linear elastic behavior up to the crushing, the contribution of FRP bars can be obtained as follows:

$$P_f = \text{£}_c' E_{fc} A_f \tag{4}$$

where A_f is the area of longitudinal FRP bars, E_{fc} is the elastic modulus of FRP bars in compression, and ε'_c is the strain of concrete at peak load. The axial capacity of the concrete specimens reinforced with GFRP bars presented in this study were calculated using the analytical procedure. The results in the form of the ratio of the analytical capacity (P_n) over the experimental value are presented in Figure 11. It shows that the analytical procedure can predict the axial capacity of the specimens very well. The prediction is a little at the safe side, which is acceptable for design applications. The figure also shows the contribution of GFRP bars (P_f) and concrete (P_c) to the ratio. It should be noted that the factor 0.85 in Equation (1) was not applied to the concrete strength as the reinforced specimens were fabricated with the same size and method of the plain specimens. Also, the proposed Equation (2) was used for the strain of reinforced concrete at the peak load. Using lower values such as conventional value of 0.002 mm/mm for the strain at peak will be more conservative.

5.2. Normalized Reinforcement Ratio

For each type of reinforcing bar used in this study, it was observed that there were similar trends within each group as the number of bars was increased. The load strain behavior up to the peak of the curve depends on the elastic modulus and reinforcement ratio. Thus, a normalized reinforcement ratio (ρ_n) for FRP-reinforced specimens was defined by multiplying the FRP reinforcement ratio (ρ_f) by the ratio of the elastic modulus of FRP reinforcement (E_f) to the elastic modulus of steel reinforcements (E_s) as follows:

$$\rho_n = \rho_f \frac{E_f}{E_s} \tag{5}$$

Figure 12 presents the experimental load capacity of the specimens versus the normalized reinforcement ratio. The figure clearly indicates a linear trend from plain to GFRP-and steel-reinforced specimens, which justify the normalized reinforcement ratio. It also indicates that

providing higher amount of GFRP bars can compensate the lack of the elastic modulus as long as a maximum reinforcement ratio criteria regarding enough space for placement of concrete is satisfied.

5.3. GFRP Bars Contribution

The contribution of GFRP bars in concrete columns have been interest of researchers and engineers. In this study, two methods were used to determine the GFRP bars contribution at peak of the test specimens and these values were averaged. The first was the force method which uses the difference between the observed load resistance (P_u) of a specimen and that which is predicted by the crushing strength of concrete (P_c) and the area of concrete in the cross-section of the specimen as follows:

$$= \frac{P_u - P_c}{P_u} \quad (6)$$

where β is the bar contribution in percent. The second method employs the elastic modulus of the bars and the strain at peak load as follows:

$$= \frac{£_c' E_{fc} A_f}{P_u} \quad (6)$$

The bar contribution at peak load of the specimens tested in this study (based on the average of the two methods) are shown in Figure 13. It observed that the bar contribution at peak is directly proportional to the normalized reinforcement ratio. For comparison, as shown in Figure 13, data from this current study was plotted alongside Fillmore and Sadeghian (2017) on smaller GFRP bars, which analyzed compressive behavior of GFRP reinforcement alongside conventional steel reinforced concrete. This external data also fit the linear relationship that was found in the current study.

In this study, the coefficient of variation (COV) of the peak load of plain, steel-reinforced, and GFRP-reinforced concrete cylinders was obtained 4.7, 1.1, and 2.5%; respectively. The average COV of bar contribution for steel and GFRP bars was calculated 0.7 and 11.2%; respectively. This shows that GFRP-reinforced specimens experienced more variability than steel-reinforced specimens. It should be noted that average strength of plain concrete was used to calculate the bar contribution of both steel- and GFRP-reinforced specimens.

Figure 13 indicates that GFRP bars contribution in the concrete cylinders is within 4.5-18.4% contribution, which is a function of its normalized reinforcement ratio ranging 0.37-1.32%. Overall, the contribution of both GFRP and steel bars shows a linear relationship with a slope of 8.5 with respect to the normalized reinforcement ration. For example, a steel reinforcement ratio of 2% will result in a bar contribution of 17%. However, the same reinforcement ratio of a GFRP bar with elastic modulus of 50 GPa (i.e. 25% of steel's elastic modulus) will result in a bar contribution of 4.2%. In conclusion, lower contribution of GFRP bars in concrete cylinders is only due to lower elastic modulus of GFRP bars with respect to steel bars.

It should be noted that the results are based on small-scale concrete cylinders and the effect of size of test specimens should be further evaluated for possible application of the results in design of large-scale concrete columns reinforced with GFRP bars. It is expected to have less contribution of GFRP bars in large-scale concrete columns. In addition, the authors are planning to test large-scale concrete columns reinforced with GFRP bars adding required data to existing data in the literature to calibrate resistance reduction factors (Phi factors) of GFRP-reinforced concrete columns for design applications.

6. CONCLUSION

In this study the effect of longitudinal GFRP bars on the behavior of axially loaded concrete cylinders was examined and benchmarked to steel reinforced and unreinforced control groups. The following conclusions can be drawn:

- In the experimental program on concrete cylinders reinforced with GFRP bars, no premature crushing of GFRPs was observed. It was shown that GFRP bars were able to sustain large strains long after the peak load of test specimens.
- Smaller modulus of GFRP bars resulted in a smaller gain in the peak load of concrete cylinders than those reinforced with steel bars. However, GFRP reinforcement results in comparable toughness and deformability for safe post-peak behaviour and resiliency.
- An analytical procedure was implemented to compute the axial capacity of GFRP-reinforced concrete cylinders. It was shown the analytical procedure can predict the axial capacity of the small-scale test specimens very well.
- GFRP bars made a meaningful contribution to the strength of concrete specimens, which was proportional to reinforcement ratio and elastic modulus. When the reinforcement ratio was normalized by multiplying it by the ratio of the elastic modulus of the reinforcement to that of conventional steel reinforcement, the axial load capacity of the test specimens was found to be a linear function.
- GFRP bar contribution in concrete cylinders under axial compression was formularized and found to be a function of its normalized reinforcement ratio within 4.5-18.4% contribution within the small-scale cylinders tested in this study.
- The results of this study showed that GFRP bars have similar elastic modulus in tension and compression, compressive strength close to two-third of tensile strength, and an appreciable

effect on the peak load resistance of concrete cylinders in uniaxial compression. Thus, neglecting the contribution of GFRP bars in compression is too conservative. However, the effect of size of test specimens should be further evaluated for possible application of the results in design of large-scale concrete columns reinforced with GFRP bars.

7. ACKNOWLEDGEMENTS

The authors are grateful for the financial support of the Natural Sciences and Engineering Research Council of Canada (NSERC) and Dalhousie University in conducting this study.

8. REFERENCES

ACI 440.1R. 2015. Guide for the Design and Construction of Structural Concrete Reinforced with Fiber-Reinforced Polymer (FRP) Bars, American Concrete Institute, Farmington Hills, MI, USA.

ACI 318. (2014). Building Code Requirements for Structural Concrete American Concrete Institute. Farmington Hills, MI, USA.

Afifi, M.Z., Mohamed, H.M. and Benmokrane, B., 2013. Axial capacity of circular concrete columns reinforced with GFRP bars and spirals. Journal of Composites for Construction, 18(1), p.04013017.

ASTM C39M-16. 2016. Standard Test Method for Compressive Strength of Cylindrical Concrete Specimens, American Society of Testing and Materials, West Conshohocken, PA, USA.

ASTM D7205/D7205M-06. 2006. Standard Test Method for Tensile Properties of Fiber Reinforced Polymer Matrix Composite Bars, American Society of Testing and Materials, West Conshohocken, PA, USA.

Bazhenov, S.L., Kuperman, A.M., Zelenskii, E.S. and Berlin, A.A., 1992. Compression failure of unidirectional glass-fibre-reinforced plastics. Composites science and technology, 45(3), pp.201-208.

Benmokrane, B., Chaallal, O. and Masmoudi, R., 1995. Glass fibre reinforced plastic (GFRP) rebars for concrete structures. Construction and Building Materials, 9(6), 353-364.

Bischoff, P.H., 2005. Reevaluation of deflection prediction for concrete beams reinforced with steel and fiber reinforced polymer bars. Journal of Structural Engineering, 131(5), pp.752-767.

CAN/CSA A23.3. 2014. Design of Concrete Structures, Canadian Standard Association. Mississauga, ON, Canada.

CAN/CSA S806-12. 2012. Design and Construction of Building Structures with Fibre-Reinforced Polymers. Canadian Standards Association, Mississauga, ON, Canada.

De Luca, A., Matta, F. and Nanni, A. 2010. Behavior of Full-Scale Glass Fiber-Reinforced Polymer Reinforced Concrete Columns under Axial Load. ACI Structural Journal, 107(5): 589-596.

Deitz, D.H., Harik, I.E. and Gesund, H., 2003. Physical properties of glass fiber reinforced polymer rebars in compression. Journal of Composites for Construction, 7(4), pp.363-366.

El-Sayed, A., El-Salakawy, E. and Benmokrane, B., 2005. Shear strength of one-way concrete slabs reinforced with fiber-reinforced polymer composite bars. Journal of Composites for Construction, 9(2), pp.147-157.

Fillmore, B. and Sadeghian, P., 2017. Compressive Behaviour of Concrete Cylinders Reinforced with Glass Fiber Reinforced Polymer Bars. Canadian Society for Civil Engineering (CSCE) Annual Conference, Vancouver, BC, Canada.

Hadhood, A., Mohamed, H.M., Ghrib, F. and Benmokrane, B., 2017. Efficiency of glass-fiber reinforced-polymer (GFRP) discrete hoops and bars in concrete columns under combined axial and flexural loads. Composites Part B: Engineering, 114, pp.223-236.

Hadi, M.N., Karim, H. and Sheikh, M.N., 2016. Experimental investigations on circular concrete columns reinforced with GFRP bars and helices under different loading conditions. Journal of Composites for Construction, 20(4), p.04016009.

Hognestad, E., 1951. Study of combined bending and axial load in reinforced concrete members. Bulletin Series No. 399, University of Illinois at Urbana Champaign, Champaign, IL, USA.

Karim, H., Sheikh, M.N. and Hadi, M.N., 2016. Axial load-axial deformation behavior of circular concrete columns reinforced with GFRP bars and helices. Construction and Building Materials, 112, pp.1147-1157.

Khorramian, K. and Sadeghian, P., 2017a. Experimental and analytical behavior of short concrete columns reinforced with GFRP bars under eccentric loading. Engineering Structures, 151, pp.761-773.

Khorramian, K. and Sadeghian, P., 2017b. Strengthening Concrete Columns using NSM CFRP Laminates. The 6th Asia-Pacific Conference on FRP in Structures (APFIS 2017), Singapore.

Khorramian, K. and Sadeghian, P., 2017c. Strengthening Short Concrete Columns Using Longitudinally Bonded CFRP Laminates. The 13th International Symposium on Fiber-Reinforced Polymer Reinforcement for Concrete Structures (FRPRCS-13), Anaheim, CA, USA.

Maranan, G.B., Manalo, A.C., Benmokrane, B., Karunasena, W. and Mendis, P., 2016. Behavior of concentrically loaded geopolymer-concrete circular columns reinforced longitudinally and transversely with GFRP bars. Engineering Structures, 117, pp.422-436.

Nanni, A., 1993. Flexural behavior and design of RC members using FRP reinforcement. Journal of structural engineering, 119(11), pp.3344-3359.

Pantelides, C.P., Gibbons, M.E. and Reaveley, L.D., 2013. Axial load behavior of concrete columns confined with GFRP spirals. Journal of Composites for Construction, 17(3), pp.305-313.

Tobbi, H., Farghaly, A.S. and Benmokrane, B. 2012. Concrete Columns Reinforced Longitudinally and Transversally with Glass Fiber-Reinforced Polymer Bars. ACI Structural Journal, 109(4): 551-558.

Tobbi, H., Farghaly, A.S. and Benmokrane, B., 2014. Behavior of concentrically loaded fiber-reinforced polymer reinforced concrete columns with varying reinforcement types and ratios. ACI Structural Journal, 111(2), p.375.

Table 1. Test matrix

Group #	ID #	Reinforcement type	Bar count	Bar size	Bar nominal diameter (mm)	Bars area (mm^2)	Reinforcement ratio (%)
1	P	None	-	-	-	0	0
2	S-4	Steel	4	10M	11.3	400	2.26
3	S-6	Steel	6	10M	11.3	600	3.40
4	S-8	Steel	8	10M	11.3	800	4.53
5	G-4	GFRP	4	#4	13	507	2.87
6	G-6	GFRP	6	#4	13	760	4.30
7	G-8	GFRP	8	#4	13	1014	5.74

Note: Three identical specimens per group were prepared and tested.

Table 2. Summary of test results

Groupe #	ID #	Normalized reinforcement ratio (%)	Peak load (kN)		Strain at peak load (mm/mm)		Toughness (N-mm/mm^3)	
			Average	SD	Average	SD	Average	SD
1	P	0.00	639.0	29.9	0.00210	0.00035	0.101	0.028
2	S-4	2.26	792.1	4.0	0.00255	0.00011	0.173	0.006
3	S-6	3.40	858.0	16.1	0.00292	0.00046	0.216	0.051
4	S-8	4.53	911.1	7.6	0.00240	0.00022	0.160	0.085
5	G-4	0.66	709.3	15.0	0.00255	0.00008	0.173	0.066
6	G-6	0.99	724.7	14.4	0.00325	0.00057	0.244	0.064
7	G-8	1.32	722.7	25.3	0.00202	0.00065	0.102	0.067

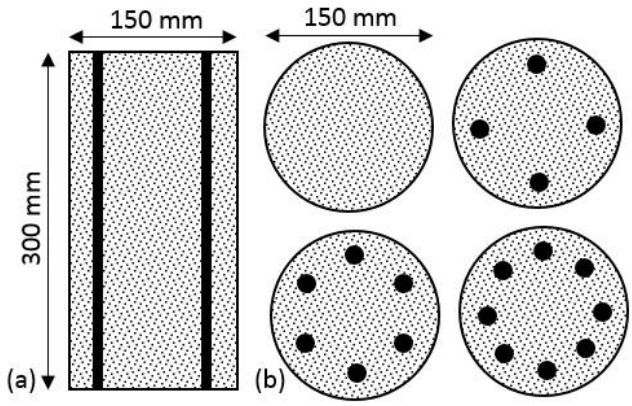

Figure 1. Specimens' geometry and reinforcing details: (a) elevation view; (b) cross-section of plain and 4-, 6-, and 8-bar specimens.

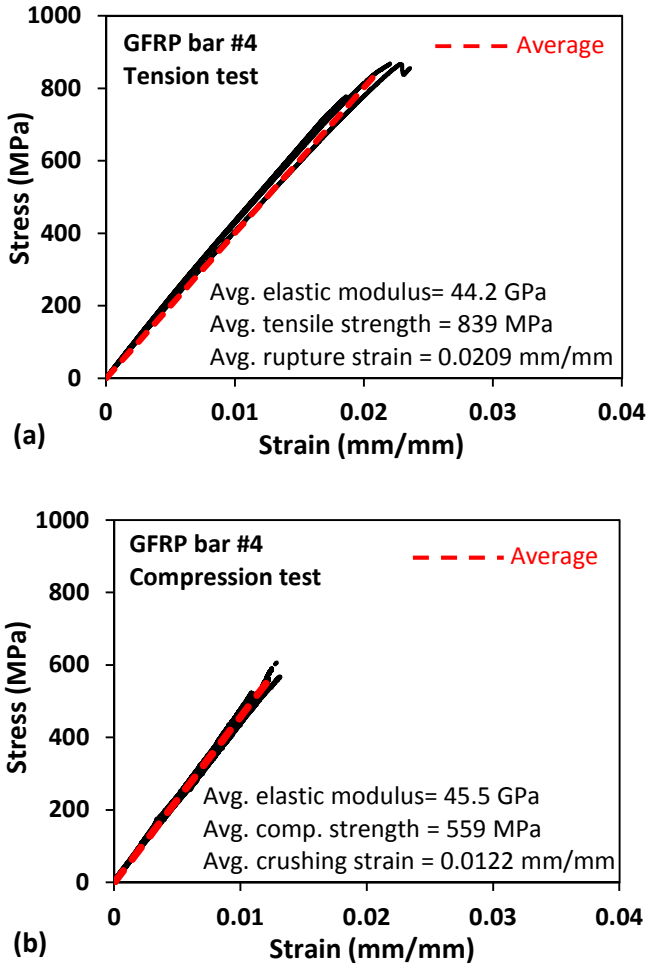

Figure 2. GFRP bar coupon test results: (a) tension; (b) compression.

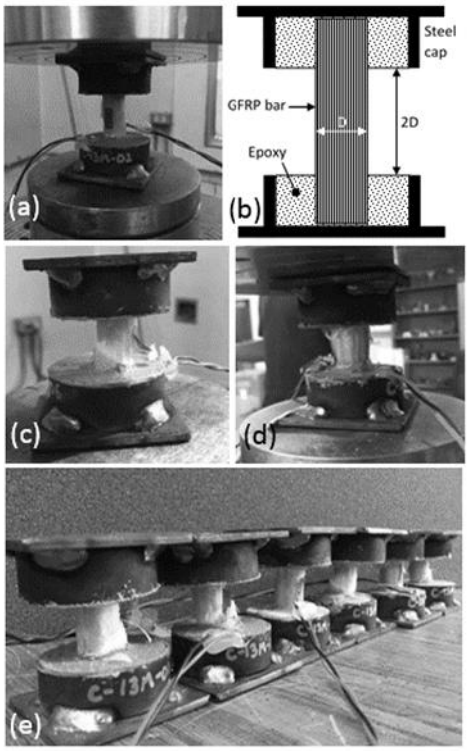

Figure 3. GFRP bar compression tests: (a) test set-up; (b) geometry of specimens; (c) diagonal crushing; (d) longitudinal splitting; and (e) all tested specimens.

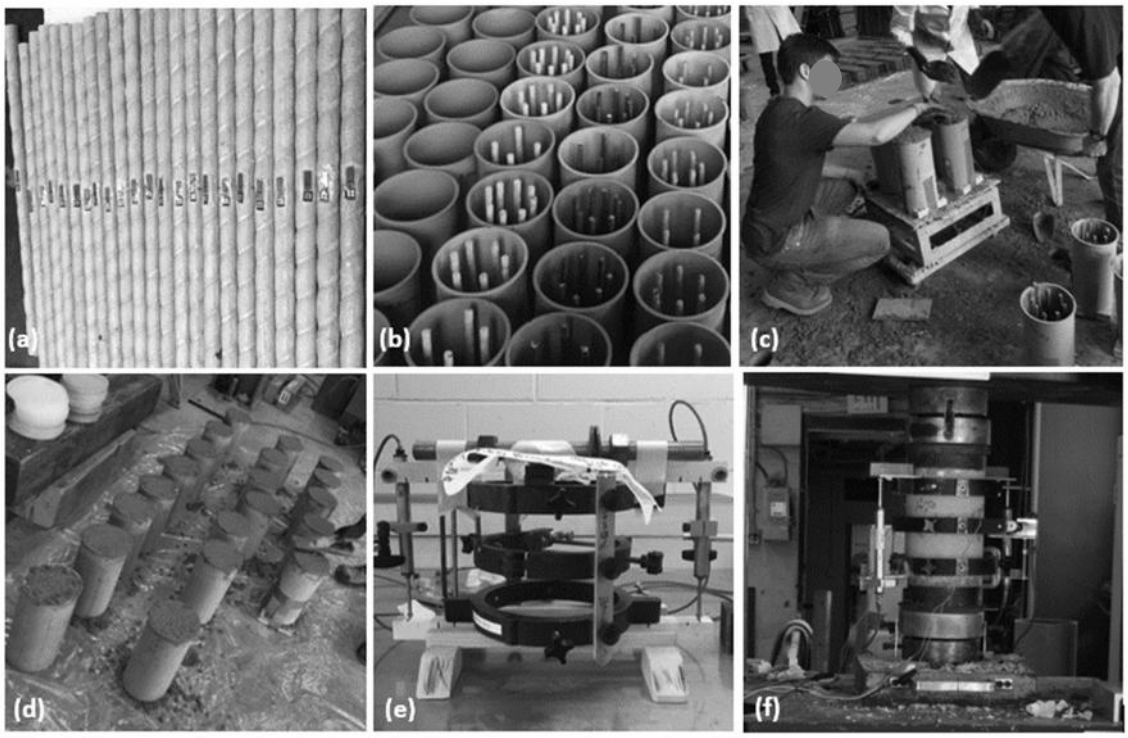

Figure 4. Specimen preparation and test set-up: (a) strain gauged bars; (b) bars installed in forms; (c) pouring concrete; (d) surface preparation; (e) external instrumentation; and (f) test set-up.

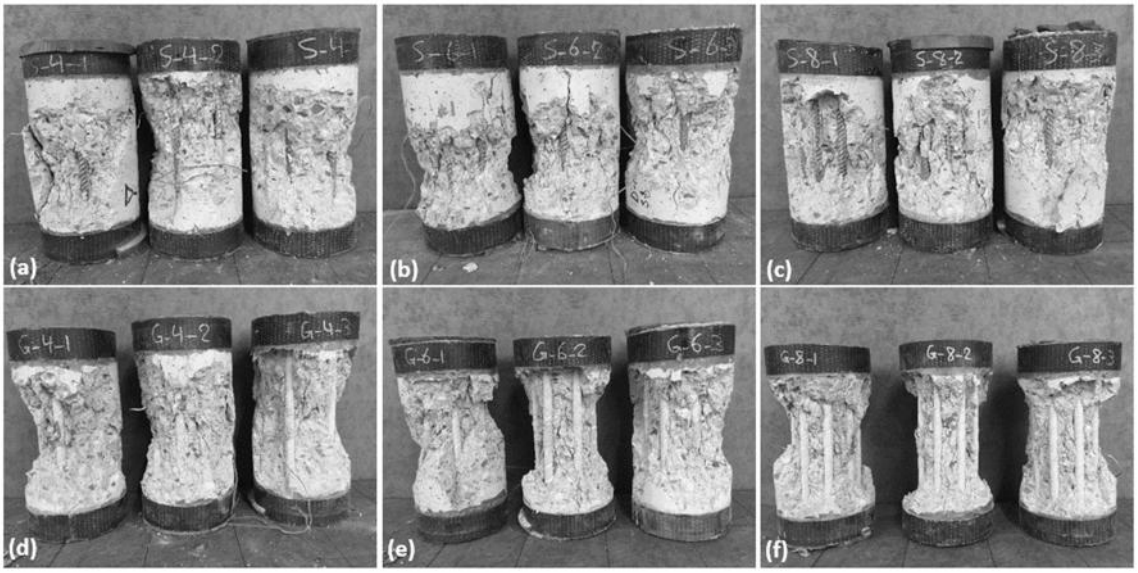

Figure 5. Tested specimens: (a) 4-bar steel S-4; (b) 6-bar steel S-6; (c) 8-bar steel S-8; (d) 4-bar GFRP G-4; (e) 6-bar GFRP G-6; and (f) 8-bar GFRP G-8.

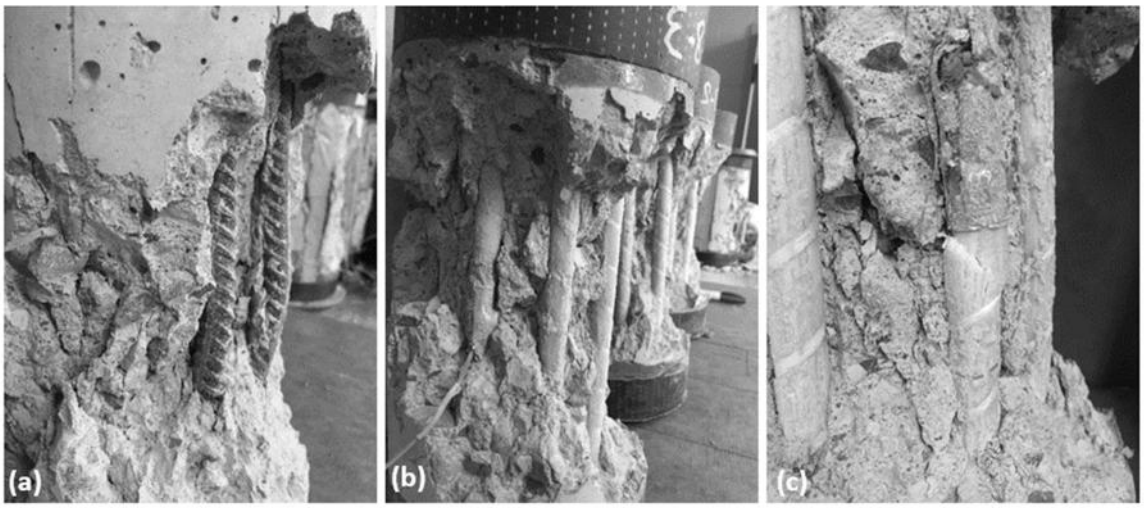

Figure 6. Failure modes: (a) inelastic buckling of steel bars; (b) elastic buckling of GFRP bars; and (c) crushing of GFRP bars.

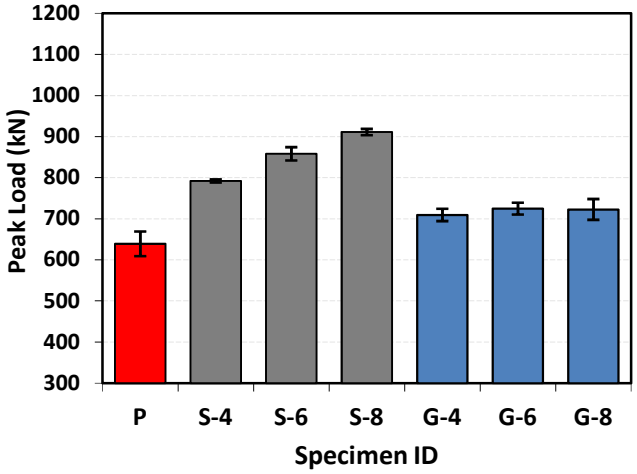

Figure 7. Effect of steel and GFRP bars on peak load (Note: each bar shows the average of three identical specimens, and error bars show the standard deviation).

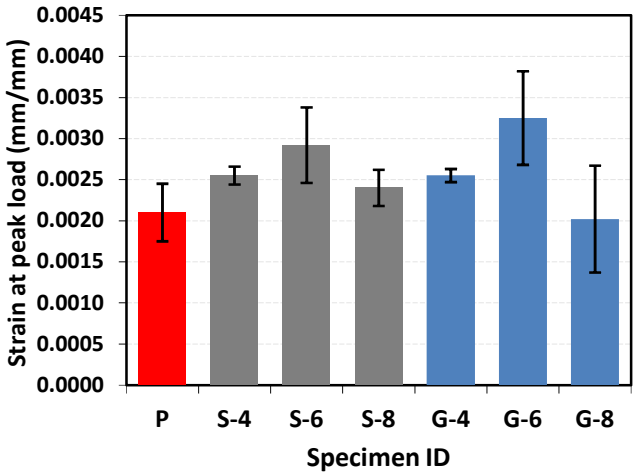

Figure 8. Effect of steel and GFRP bars on axial strain at peak load.

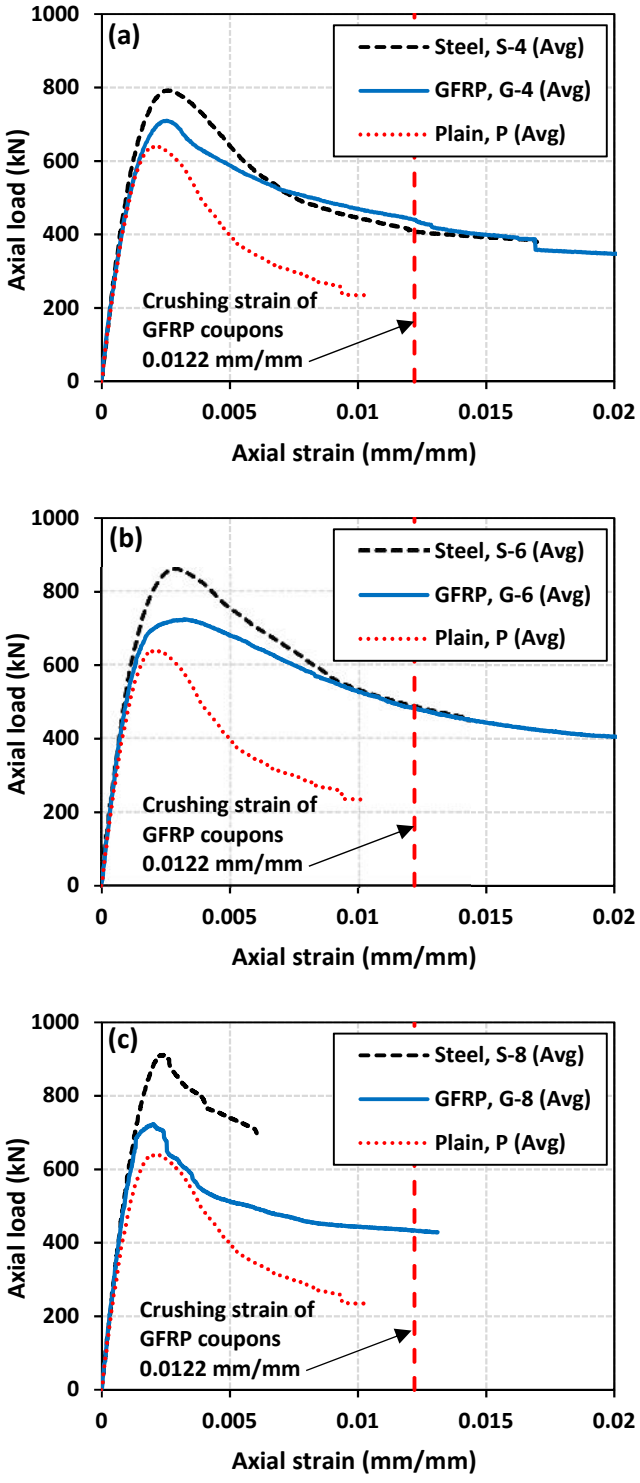

Figure 9. Axial load-axial strain curves of test specimens: (a) 4-bar groups; (b) 6-bar groups; and (c) 8-bar groups (Note: each curve is average of three identical specimens. Two strain gauges were used to obtain strain values of each specimens).

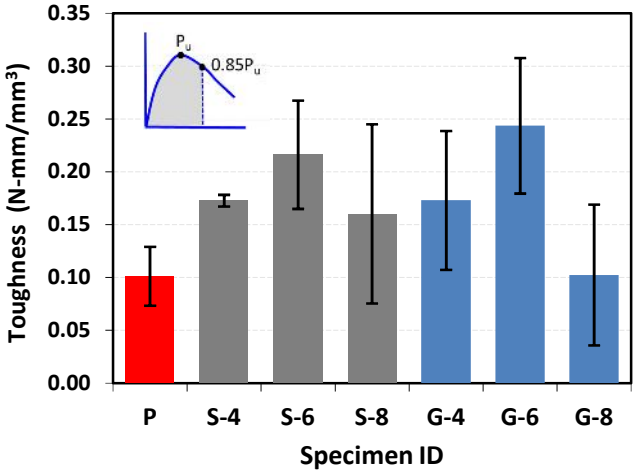

Figure 10. Effect of steel and GFRP bars on toughness.

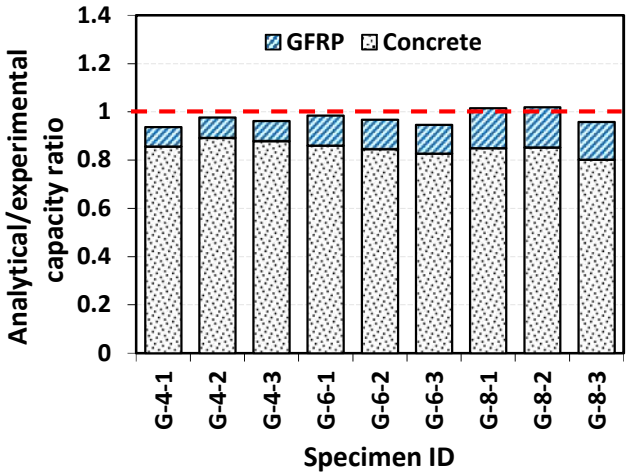

Figure 11. Analytical/experimental axial capacity ratio of concrete cylinders reinforced with GFRP bars (Note: contribution of concrete and GFRP bars in analytical model are shown).

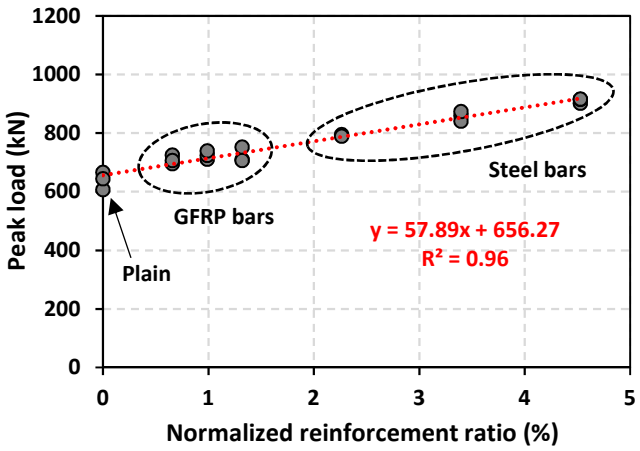

Figure 12. Peak load vs. normalized reinforcement ratio

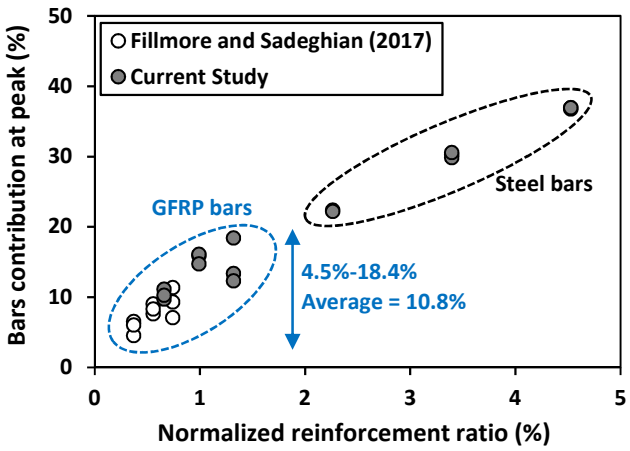

Figure 13. Comparison of steel and GFRP bar contribution to axial capacity of concrete cylinders at peak load.